

## Layer-by-layer epitaxial thin films of the pyrochlore $Tb_2Ti_2O_7$

This content has been downloaded from IOPscience. Please scroll down to see the full text.

2017 Nanotechnology 28 055708

(<http://iopscience.iop.org/0957-4484/28/5/055708>)

View [the table of contents for this issue](#), or go to the [journal homepage](#) for more

Download details:

IP Address: 128.41.61.111

This content was downloaded on 09/02/2017 at 14:17

Please note that [terms and conditions apply](#).

You may also be interested in:

[Investigations of the effect of nonmagnetic Ca substitution for magnetic Dy on spin-freezing in  \$Dy\_2Ti\_2O\_7\$](#)

V K Anand, D A Tennant and B Lake

[Structural and magnetic properties of single-crystals of the geometrically frustrated zirconium pyrochlore,  \$Pr\_2Zr\_2O\_7\$](#)

M Ciomaga Hatnean, C Decorse, M R Lees et al.

[Quantum spin ice: a search for gapless quantum spin liquids in pyrochlore magnets](#)

M J P Gingras and P A McClarty

[Bulk magnetization of the heavy rare earth titanate pyrochlores - a series of model frustrated magnets](#)

S T Bramwell, M N Field, M J Harris et al.

[Crystal structure and strain state of molecular beam epitaxial grown  \$Gd\_2O\_3\$  on  \$Si\(1\ 1\ 1\)\$  substrates](#)

J X Wang, A Laha, A Fissel et al.

[Resonant x-ray diffraction revealing chemical disorder in sputtered  \$L\_{10}FeNi\$  on  \$Si\(001\)\$](#)

Andreas Frisk, Bengt Lindgren, Spiridon D Pappas et al.

[Effect of Ising-type  \$Tb^{3+}\$  ions on the low-temperature magnetism of La, Ca cobaltite](#)

K Knížek, Z Jirák, J Hejtmánek et al.

[Magnetotransport and magnetothermal properties of the ternary intermetallic compound  \$TbFe\_2Al\_{10}\$](#)

Ashish Khandelwal, M K Chattopadhyay and S B Roy

# Layer-by-layer epitaxial thin films of the pyrochlore $\text{Tb}_2\text{Ti}_2\text{O}_7$

Laura Bovo<sup>1</sup>, Christopher M Rouleau<sup>2</sup>, Dharmalingam Prabhakaran<sup>3</sup> and Steven T Bramwell<sup>1,4</sup>

<sup>1</sup> University College London, London Centre for Nanotechnology, 17–19 Gordon Street, London WC1H 0AH, UK

<sup>2</sup> Center for Nanophase Materials Sciences, Oak Ridge National Laboratory, Chestnut Ridge Drive, Oak Ridge, TN 37831 USA

<sup>3</sup> Department of Physics, University of Oxford, Clarendon Laboratory, Parks Road, Oxford, OX1 3PU, UK

<sup>4</sup> University College London, Department of Physics & Astronomy, Gower St, London WC1E 6BT, UK

E-mail: [l.bovo@ucl.ac.uk](mailto:l.bovo@ucl.ac.uk)

Received 31 August 2016, revised 23 November 2016

Accepted for publication 1 December 2016

Published 29 December 2016



CrossMark

## Abstract

Layer-by-layer epitaxial growth of the pyrochlore magnet  $\text{Tb}_2\text{Ti}_2\text{O}_7$  on the isostructural substrate  $\text{Y}_2\text{Ti}_2\text{O}_7$  results in high-quality single crystal films of up to 60 nm thickness. Substrate-induced strain is shown to act as a strong and controlled perturbation to the exotic magnetism of  $\text{Tb}_2\text{Ti}_2\text{O}_7$ , opening up the general prospect of strain-engineering the diverse magnetic and electrical properties of pyrochlore oxides.

Keywords: epitaxial thin films,  $\text{Tb}_2\text{Ti}_2\text{O}_7$ , frustrated magnets, RHEED-PLD, strain engineering

(Some figures may appear in colour only in the online journal)

## Introduction

Compared to bulk phases, epitaxial oxide films can show superior properties with advantages that include high purity, abrupt interfaces, and high structural uniformity. For example, epitaxial thin films with ferromagnetic, ferroelectric or multiferroic properties have played a crucial role in developing a new generation of spin-electronic devices [1–3], while epitaxial perovskite oxides have shown enhanced catalytic performance for application as cathodes in fuel cells as compared to their powder counterparts [4–7]. In both of these instances, thin-film growth techniques have allowed the properties of existing materials to be modified and tailored by strain engineering.

A significant class of oxide material that has been studied only recently in thin film form [8–11] is that having the pyrochlore structure type, with general formula  $\text{A}_2\text{B}_2\text{O}_7$  [12]. Here the A and B cations typically occupy separate

interpenetrating lattices of corner sharing tetrahedra. The preparation of pyrochlore thin films has been motivated by interest in the unusual magnetic and electrical properties of the series [12]. Thus,  $\text{Dy}_2\text{Ti}_2\text{O}_7$  [8] and  $\text{Ho}_2\text{Ti}_2\text{O}_7$  [9] have been studied for their spin ice behaviour,  $\text{Bi}_2\text{Pt}_2\text{O}_7$  as a candidate fuel cell cathode material [10], and pyrochlore iridates as candidate topological materials [11].

We recently reported [8] the first epitaxial films of the spin ice  $\text{Dy}_2\text{Ti}_2\text{O}_7$  grown on the non-magnetic pyrochlore substrate  $\text{Y}_2\text{Ti}_2\text{O}_7$ . One of our main findings was that the spin ice behaviour of the bulk was altered significantly by substrate-induced strain [8], a result that recommends the use of inert pyrochlore substrates as a method of perturbing and probing the fascinating magnetic properties of pyrochlores in a controlled manner. Thin film spin ices represent a new approach to ice-type magnetic systems that complements classical and quantum spin ice in the bulk [13–15] as well as artificial spin ice micromagnetic arrays [16–20].

In this paper, we report the preparation and characterization of the first epitaxial thin films of  $\text{Tb}_2\text{Ti}_2\text{O}_7$  (TTO) which, as in our previous work [8], were grown on  $\text{Y}_2\text{Ti}_2\text{O}_7$  (YTO) substrates. TTO is a relative of spin ice with particularly unusual magnetic properties, that remain mysterious

 Original content from this work may be used under the terms of the [Creative Commons Attribution 3.0 licence](https://creativecommons.org/licenses/by/3.0/). Any further distribution of this work must maintain attribution to the author(s) and the title of the work, journal citation and DOI.

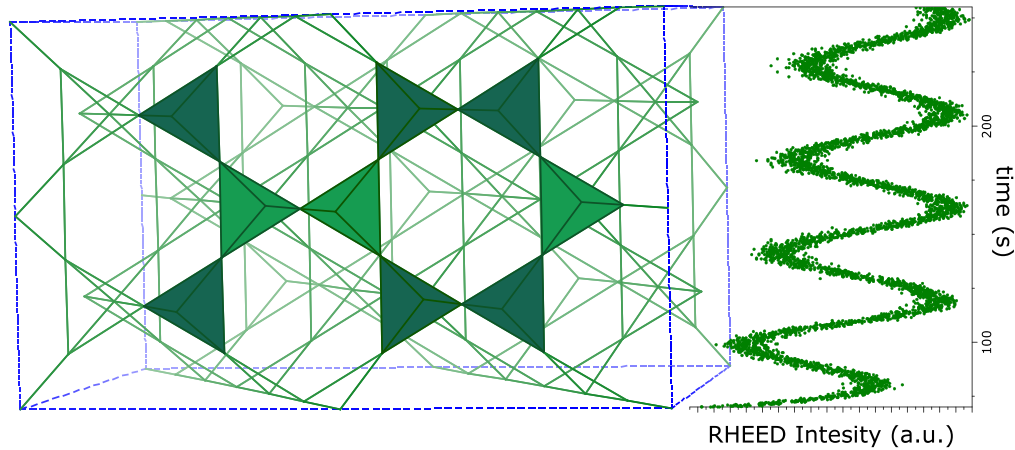


**Figure 1.** Layer-by-layer epitaxial growth. A schematic representation of the detected growth mechanism along the out-of-plane direction [110]. Each RHEED oscillation corresponds to the formation of one tetrahedral layer (a quarter of the unit cells). The network shows the pyrochlore structure with highlighted tetrahedra.

**Table 1.**  $x$ TTO||YTO(110): list of samples with  $x$  indicating the number of monolayers.

Sample	Pulses	Thickness (fringes) nm	Thickness (reflectivity) nm	Thickness (RHEED) nm	Density (reflectivity) $\text{g cm}^{-3}$
YTO	Annealed substrate	—	—	—	—
$x = 63$	7512	62.6(1)	62.7(1)	62.2(2)	6.9(2)
$x = 11$	1252	10.4(1)	10.3(1)	10.4(2)	6.8(2)
$x = 5$	626	5.2(1) <sup>a</sup>	5.4(1)	5.2(2)	7.1(2)

<sup>a</sup> This thickness value has been extrapolated from the number of pulses.

despite many years of research [21–26]. It fails to order magnetically down to  $T = 50$  mK, instead forming a spin liquid [14], possibly governed by ice rules [27–30], magnetoelastic effects [26], and quantum fluctuations [15, 23, 31]. The ground electronic state of the  $\text{Tb}^{3+}$  ion is an approximate doublet, with a more precisely defined doublet at  $\sim 15$  K above the ground term. Formulation of the single ion and collective spin Hamiltonian has developed around at least two competing models [24, 25]. An early and striking result on TTO was the ‘crystallization’ of the spin liquid under strong applied pressure [22]. In this context, it is particularly interesting to examine the properties of TTO on YTO as epitaxial strain would be expected to significantly perturb the properties of the bulk.

## Results and discussion

The single crystal epitaxial films of TTO were deposited on isostructural YTO, both cubic pyrochlores, space group  $Fd\bar{3}m$ , lattice constant  $a = 1.0152, 1.0083$  nm, respectively. The substrates were prepared, cut and aligned as described in methods. Three set of films were made, of thickness 5 nm, 11 nm and 63 nm respectively (note that  $1 \text{ nm} \cong 1$  monolayer)—details of these samples are reported in table 1. In each the out-of-plane direction is  $(1\bar{1}0)$ , with  $(111)$  and  $(11\bar{2})$  forming orthogonal directions in-plane, parallel to the substrate edges. Use of the non-commercial substrate YTO had already proven to be an advantage in obtaining very high

quality thin epitaxial layers with the pyrochlore structure [8]. In the present study, we were further able to determine a layer-by-layer growth mechanism by following the characteristic intensity oscillation of the reflection high-energy electron diffraction (RHEED); a schematic representation is reported in figure 1, with more details given further down the text. Similar behaviour may be anticipated for other pyrochlores grown under similar conditions, opening up the exciting prospect of creating multilayers, heterostructures, and interfaces of pyrochlore materials with atomic-layer precision.

Figure 2(a) displays the out-of-plane 440 x-ray reflection, recorded for three different film thicknesses. The out-of-plane lattice parameters are  $1.025(1)$  nm and  $1.009(1)$  nm for the films and substrate, respectively. The thickness of each sample was determined from the fringes observed in the XRD pattern, as well as by fitting reflectivity curves (figure 2(b)); these results are summarized in table 1, columns 3 and 4. The main purpose of the reflectivity analysis was to estimate the thickness and the density of the film, both of which are expected to be reliable numbers in our analysis. The calculated total thicknesses are in close agreement with the values calculated on the basis of the number of laser pulses used during the growth. Furthermore, the density of the film is close to the tabulated bulk density of  $\text{Tb}_2\text{Ti}_2\text{O}_7$  (table 1). Two orthogonal off-specular reflections have been measured and figure 3 shows both of them for the thicker sample 63TTO||YTO(110) (in this notation [8] the number of monolayers is indicated on the left and the crystallographic face on the

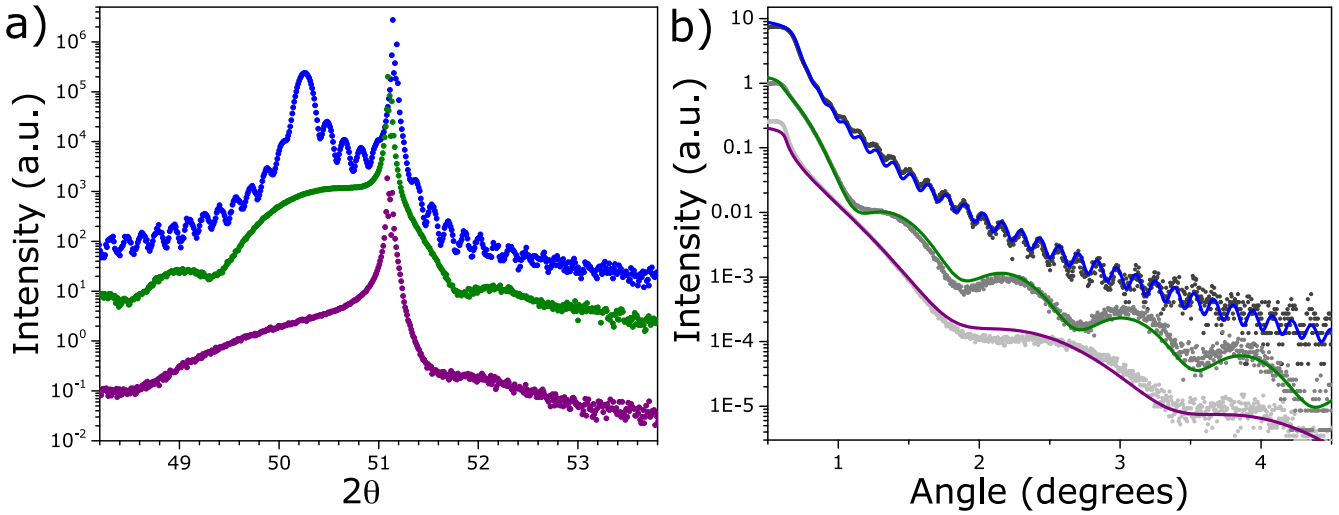


**Figure 2.** First TTO films. Room temperature structural properties of  $\text{Tb}_2\text{Ti}_2\text{O}_7 \parallel \text{Y}_2\text{Ti}_2\text{O}_7(110)\text{K}(111)$ . Colour code:  $x\text{TTO} \parallel \text{YTO}(110)$  with  $x = 63$  (blue),  $x = 11$  (green),  $x = 5$  (purple),  $x$  indicating the number of monolayers. (a) High resolution  $2\theta - \omega$  scans showing (440) reflection for different film thicknesses. (b) Reflectivity measurements and related fits. In both plots, each scan has been displaced vertically to improve clarity.

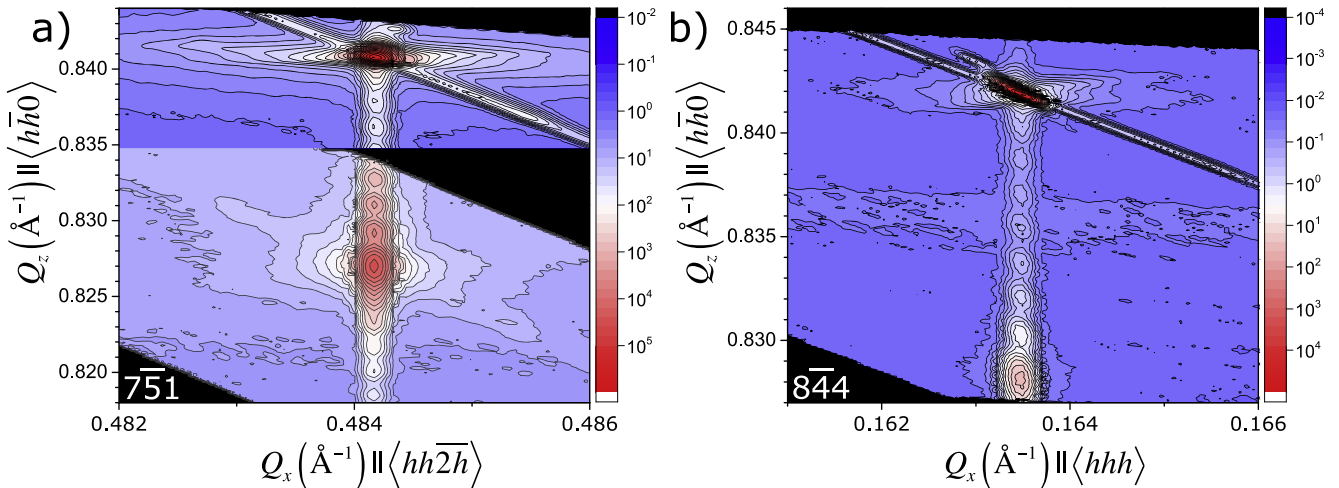
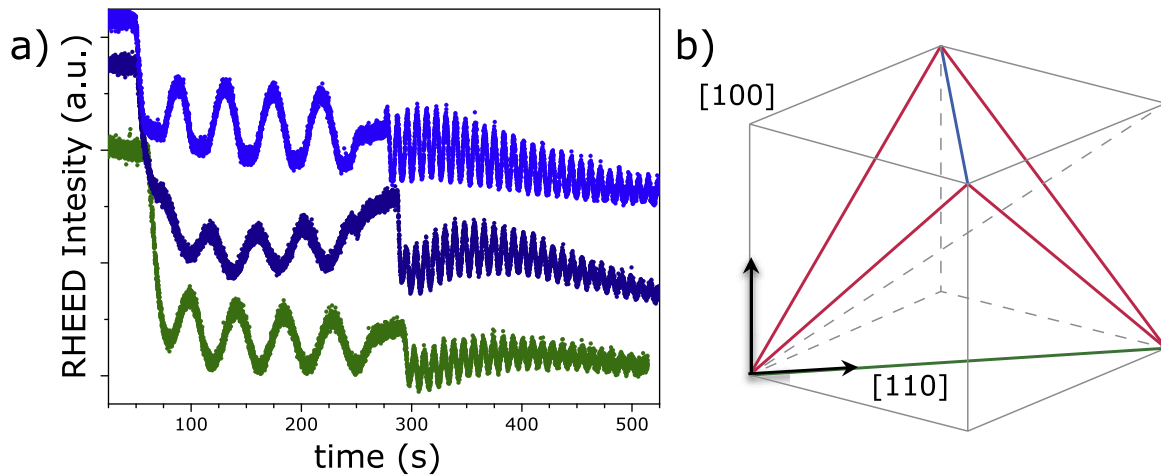


**Figure 3.** Epitaxy and compressive strain. Room temperature high-resolution XRD reciprocal space maps (RMS) showing (a)  $(7\bar{5}1)$  and (b)  $(8\bar{4}4)$  reflections for  $63\text{TTO} \parallel \text{YTO}(110)$ . Here, the two orthogonal  $Q_x$  are the components of the reciprocal space vector aligned with the substrate in-plane edges. These RMS confirm the film is high quality, fully epitaxial, and fully strained along the two in-plane orientations.

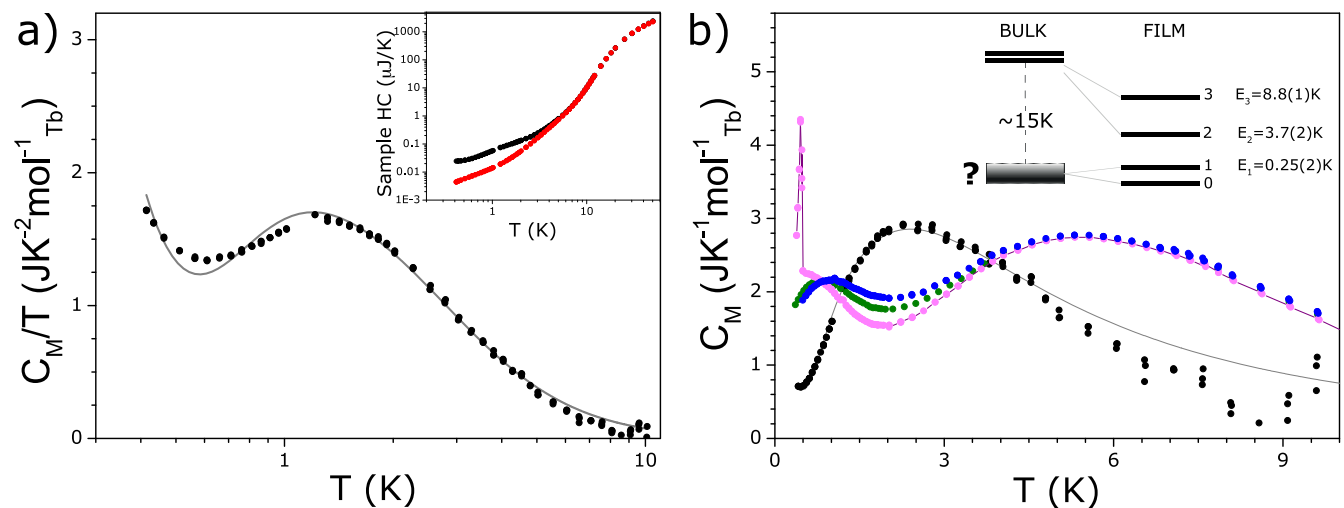
right). These measurements show the films are very uniform (clear fringes appear in both spectra) and that they have a compressive strain, consistent with the smaller lattice constant of the substrate.

Figure 4(a) is as an example of a RHEED pattern that was recorded during the depositions, and the oscillation period measured at the specular reflection turns out to be compatible with the formation of a quarter of the unit cell along the out-of-plane direction  $[110]$ ; see also the schematics in figure 1. Along this crystallographic direction, each pyrochlore unit cell contains four corner-shared tetrahedra of the Tb sub-lattice; one RHEED oscillation corresponds to the formation of one tetrahedral layer. The thickness calculated from this model is in excellent agreement with the XRD analysis (table 1).

It is interesting to examine the lattice distortion in more detail, as this affects the distance between the Tb ions and their oxide environment (hence the magnetic moments, and their hamiltonian) and will most certainly have an impact on the magnetic properties of the thin films. Figure 4(b) shows a schematic of one Tb tetrahedron and its orientation with respect to the cubic pyrochlore axis. In the *cubic* phase, all Tb–Tb distances are *equal*:  $d_{\text{Tb}} = 3.589 \text{ \AA}$  for a lattice constant of 1.0152 nm. Analysis of the diffraction data indicates that the epitaxial strain is homogenous, the film structure being compressed equally along  $(111)$  and  $(11\bar{2})$ , with the average density maintained by elongation along the  $(1\bar{1}0)$  direction. When looking at the Tb sub-lattice, one finds that not all the distances are equivalent: in particular, the  $(1\bar{1}0)$  and  $(110)$  (green and blue lines in figure 4(b),



**Figure 4.** (a) Layer-by-layer growth. Reflection high-energy electron diffraction (RHEED) oscillations measured at the specular spot during deposition. Three different growths are shown to confirm reproducibility. Two repetitions rate were used during each deposition (initial 200 pulses at 1 Hz to help nucleation, increased to 5 Hz afterwards), hence the two oscillation periods. One oscillation corresponds to  $\frac{1}{4}$  of the cell, equivalent to the formation of one tetrahedron of Tb ions (one unit cell along the [110] orientation contains four corner shared tetrahedra of Tb ions). (b) Structural distortion. Schematic of the Tb sub-lattice is shown, where the tetrahedra edges depict the Tb–Tb distances. In the pyrochlore *cubic* structure these are all identical ( $d_{\text{Tb}} = 3.589 \text{ \AA}$  for lattice parameter of 1.0152 nm). In the  $x\text{TTO}||\text{YTO}(110)$  strained film, the [110] (green) measures  $d_{(110)} = 3.627 \text{ \AA}$ ; the  $[1\bar{1}0]$  (blue)  $d_{(1\bar{1}0)} = 3.567 \text{ \AA}$  and the remaining four distances (red) measure  $d_{\text{other}} = 3.582 \text{ \AA}$ .



**Figure 5.** Specific heat and energy levels. Data for 63TTO||YTO(110). (a) Insert shows the raw scans of the thin layer (black) and the annealed YTO substrate (red): a clear difference is detected below 10 K due to the presence of the TTO epitaxial layer. (a) Magnetic contribution and related fit. The quantity  $C_M/T$  is plotted after subtraction of the substrate and lattice contributions (see main text). The line is a fit to a four singlet levels (adjusting three energies only): energy level diagram is depicted in panel (b) insert. (b) Comparison with bulk TTO. Green, blue and pink dots are previously reported [36–38] single crystal data (pink line is just a guide to the eye). The specific heat profile of TTO thin film is drastically different than of the bulk.

respectively) distances measure  $d_{(1\bar{1}0)} = 3.567 \text{ \AA}$  and  $d_{(110)} = 3.627 \text{ \AA}$ , respectively, and the other four measure  $d_{\text{other}} = 3.582 \text{ \AA}$  (red lines in figure 4(b)). The angles between the tetrahedron edges are perturbed accordingly. With homogenous strain, the space group symmetry is reduced to orthorhombic,  $A1$ , with a six-fold increase in the number of atoms per unit cell. Despite the large unit cell, it is reasonable to expect a single local environment for the  $\text{Tb}^{3+}$  ions, and our analysis of the magnetic and thermal properties assumes this. However, a complete description of

the crystal structure must await a detailed analysis by synchrotron x-ray techniques.

The thicker sample 63TTO||YTO(110) was chosen as a prototype to investigate the magnetic behaviour of the epitaxial layers. Its relative thickness gives the advantage of minimizing the difficulties in quantitatively separating the contribution of the active material (TTO) from that of the substrate (YTO). The extension of the analysis to thinner films requires a much more extensive and accurate study that is beyond the scope of the present work.

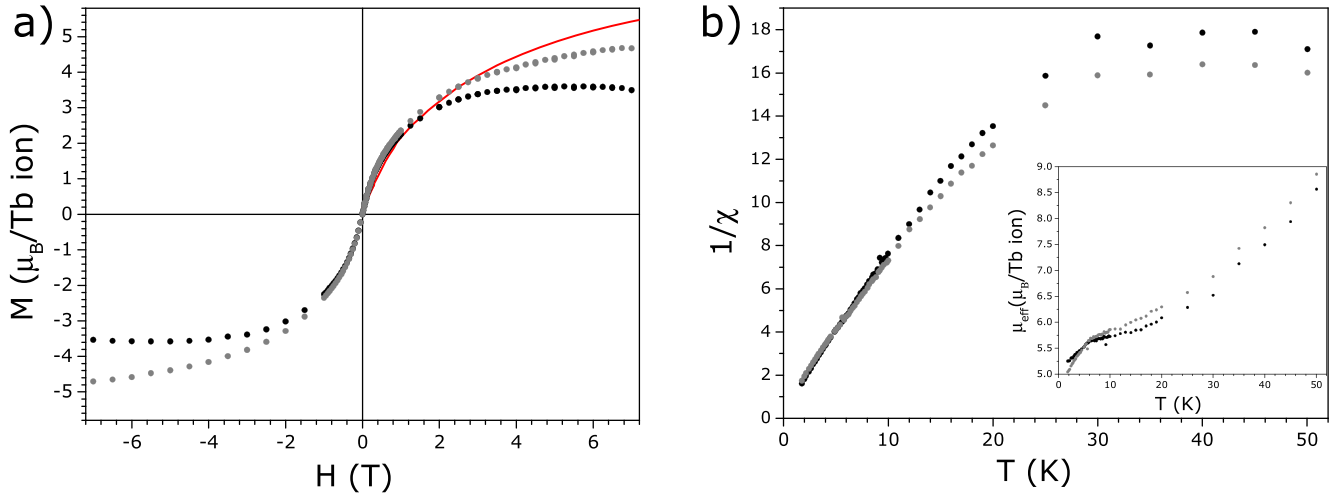


**Figure 6.** (a) Magnetization versus field curves measured at 1.8 K for 63TTO||YTO(110) along the two in-plane orthogonal orientations [111] (grey) and [112] (black); data have been subtracted for the substrate contribution. As a comparison, digitized data [34] for a powder TTO sample are reported. The anisotropy shown is in line with that of Ising magnetic moments confined to point parallel or antiparallel to their local [111] directions. Initial slope of the two curves give a magnetic moment of  $\mu_{\text{eff}} = 5.4 \pm 0.2 \mu_B$ . (b) Susceptibility reported in the dimensionless SI units measured at low magnetic field (0.02 T) and its temperature dependence. The anisotropy vanishes in the limit of linear susceptibility as shown by our data. The insert reports the effective magnetic moment versus  $T$ .

A commercial PPMS system (see methods) was used to measure the heat capacity of the TTO thin films, taking advantage of our previous demonstration [8, 32] that the PPMS can be used to accurately measure the heat capacity of pyrochlore thin films. Figure 5(a) reports an overview of the low temperature specific heats of 63TTO||YTO(110) and the annealed substrate YTO(110), and as clearly shown in the insert of figure 5(a), there is a distinct contribution in the raw data from the thin layer of TTO at temperatures below 10 K. To estimate the magnetic specific heat of the film,  $C_M$ , the measured heat capacity was corrected for the contributions from substrate and phonons using the same method described at length in [8].

The magnetic specific heat,  $C_M$ , divided by temperature is plotted in figure 5(a). In a single-ion approximation, by comparison with the bulk, we expect up to four microstates to be thermally active. Considering all models with four microstates we found that  $C_M(T)$  is uniquely and quantitatively described by a system of four singlets, with the first excited singlet at  $E_1 = 0.25(2)\text{K}$ ; followed by  $E_2 = 3.7(2)\text{K}$  and  $E_3 = 8.8(1)\text{K}$ . The grey line in figure 5(a) is a fit to this four level system where the only fitting parameters being the three energy values reported above. The quantitative accuracy of the single ion description, coupled with the well-defined x-ray diffraction and RHEED oscillations, rules out any significant role of sample imperfection. As in the case of the bulk [21], and in contrast to the case of applied pressure [22], there is no transition to range order evident down to 0.4 K. The modest departure from the single-ion model evident in figure 5(a) at low temperature is suggestive of weak exchange and dipole interactions that perturb the single ion states.

This behaviour may be compared to that of bulk TTO. In that case, it is accepted that an excited doublet lies close the ground doublet (at about 15–18 K) [33, 34], and both of these can have their degeneracies lifted by Jahn–Teller distortions

[35]. The bulk specific heat can be fitted to a single ion model with the ground state doublet split by 1.8 K into two singlets [24]. Following a debate [24, 25], it was established that these excitations are in fact dispersive [30], with quadrupolar interactions and coupling with phonons playing a role. However, sample imperfection in bulk crystals complicates interpretation of the specific heat [36–38] as shown in figure 5(b), where data for three different bulk TTO crystals are presented (taken from [36–38]). The peak near 6 K is attributed to the first excited doublet, whereas the origin of the signal(s) below 3 K is the subject of debate [24, 25]. The contrast with the specific heat of the film is striking, yet it can be understood in terms of the high sample quality gained by layer-by-layer deposition (thereby clarifying the low temperature behaviour) and the removal of crystal field degeneracy by epitaxial strain. Figure 5(b) shows a schematic of the energy levels and how they vary when passing from bulk to thin film. We note that in the future it may be possible to use substrates with tailored lattice constants to extrapolate the evolution of the electronic state back to *unstrained* and *near-perfect* TTO, thereby settling the issue of its *true* electronic state, definitively [24, 25, 30].

To further compare the film with the bulk, magnetization and magnetic susceptibility were measured, and figure 6 summarizes our findings. These data have been corrected for a paramagnetic contribution arising from defects in YTO, quantitatively estimated by direct measurement of the annealed substrate. Digitized [34] data for a powder sample are reported for comparison, and it can be observed that the magnetization of the thin film is in close agreement with that of bulk TTO. The two orthogonal crystallographic orientations show the anisotropy expected for Ising spins constrained to the local [111] local direction [39, 40]; the moment ratio between the [111] and [112] directions approaches the expected value of 1.3 at 7 T. From the slope of the

magnetization versus field curves measured at 1.8 K, we extrapolate an effective moment  $\mu_{\text{eff}} = 5.4 \pm 0.2 \mu_B$ ; this is in close agreement with the calculated magnetic moment associated with the ground state of bulk TTO [33, 34]. Figure 6(b) reports the magnetic susceptibility of 63TTO||YTO(110), measured at low field as a function of temperature; the inset shows the evolution of the effective moment  $\mu_{\text{eff}}$  versus temperature. Looking at the effective moment, one can see that at  $T = 2$  K it resembles that associated with the ground state bulk TTO [33, 34]. It then rather quickly increases to  $\mu_{\text{eff}} = 5.9 \pm 0.2 \mu_B$  close to  $T = 10$  K, but again it is in close agreement with the moment associated with the first excited doublet in bulk TTO [33]. Subsequently, the magnetic moment increases more slowly with temperature, finally approaching the free ion value.

A detailed understanding of these magnetic moments in the context of the four singlet levels inferred from specific heat must await a quantitative analysis of the crystal field hamiltonian. Although singlet states are non-magnetic to first order in magnetic field, higher order Zeeman splittings can be difficult to distinguish from first order ones in bulk magnetization measurements. Hence the observed magnetic moments, while suggesting doublet levels, should not be thought of as necessarily being inconsistent with a singlet structure. However, it is also possible that the inferred singlet states are not true single ion states, but instead reflect peaks in a density of states.

What seems certain is that our TTO films represent an improvement in sample quality over the bulk and that the experimental properties of our films present a clear picture that any theory of TTO must seek to encompass. This means that the epitaxial strain in the films may be used as a systematic probe of interactions in the bulk. For example, there is likely to be a coupling between the strain and single ion quadrupoles [30] and hence the films can be used to investigate this.

## Conclusion

In conclusion, TTO is part of a family of pyrochlores with exotic magnetic properties: relatives so far unstudied in thin film form include  $\text{Yb}_2\text{Ti}_2\text{O}_7$ , which is a candidate *quantum spin ice*, and  $\text{Er}_2\text{Ti}_2\text{O}_7$ , the leading candidate for magnetic *order-by-disorder* [12, 15]. Our study identifies a new way of probing and perturbing such systems, and alleviating problems of sample quality. More generally, our study suggests that pyrochlore oxides may be excellent subjects for forming heterostructures, thereby opening broad possibilities for tailoring and exploiting the diverse magnetic and electronic properties of the pyrochlore series.

## Methods

### Pulsed laser deposition (PLD)

Single crystals of  $\text{Y}_2\text{Ti}_2\text{O}_7$  [41] were cut and epi-polished on one side (SurfaceNet GmbH, <http://surfacenet.de>). A set of

fully oriented YTO substrates was prepared: YTO110K111, where the first crystallographic direction (hkl) is the out-of-plane orientation and the second (Khkl) identify one of the in-plane edges of the square substrate. Epitaxial TTO thin films (between 65 and 5 nm in thickness) were grown on YTO substrates by pulsed laser epitaxy (KrF,  $\lambda = 248$  nm) at 750 °C in 113 mTorr  $\text{O}_2$ . The laser fluence at the target was fixed at  $1.97 \text{ J cm}^{-2}$ ; the laser repetition rate was initially set at 1 Hz for the first 200 shots and increase to 5 Hz for the remaining growth. Samples were subsequently post-annealed for 1 h at 750 °C in 400 Torr  $\text{O}_2$  before cooling down to room temperature. RHEED was used to monitor the surface structure and to control the film thickness with atomic-layer precision.

### Structural characterization

Lattice parameters and film epitaxy were studied at room temperature by XRD using  $\text{Cu K}\alpha 1$  radiation in a Rigaku high-resolution diffractometer. Film thickness was determined by x-ray reflectivity; the fits were performed with the Integrated Thin Film Analysis Software GlobalFit 1.3 (Rigaku Corporation). High-resolution reciprocal space maps were collected using the same machine.

### Magnetic properties

In-plane magnetization was measured using a Quantum Design MPMS-7 SQUID (superconducting quantum interference device) magnetometer. Measurements were performed in RSO (reciprocating sample option); silver dag was removed from the underside of samples to prevent the possibility of spurious magnetic signals attributed to material from the heater block of the deposition system. Samples were positioned using a customized sample holder to avoid displacement or reorientation during the measurement. Finally, the holder was loaded inside a clear plastic straw having a 5 mm inside diameter. This arrangement allows complete cancellation of background signals from the sample holder and strongly reduces the effect of field noise in the magnet.

### Specific heat

The specific heat of each sample was measured from 50 and 0.4 K with a Quantum Design PPMS (physical properties measurement system) with a  $^3\text{He}$  option.

## Acknowledgments

PLD deposition of the thin films was conducted by LB and with assistance from CMR at the Center for Nanophase Materials Sciences, which is a DOE Office of Science User Facility (CNMS2015-251). LB is supported by The Leverhulme Trust through the Early Career Fellowship program (ECF2014-284). DP acknowledges support from the EPSRC grant EP/K028960/1. The Authors thanks M J P Gingras for useful discussions and related collaborations.

## Author Contributions

LB and STB conceived the project. DP prepared the target for PLD deposition and grew the crystals used to obtain substrates. PLD deposition of the thin films was conducted by LB with assistance from CMR. LB performed all the experiments and analysed the data. LB and STB discussed and interpreted the results; they drafted the manuscript and incorporated suggestions from the co-authors.

## References

- [1] Ramesh R and Spaldin N A 2007 Multiferroics: progress and prospects in thin films *Nat. Mater.* **6** 21
- [2] Opel M 2012 Spintronic oxides grown by laser-MBE *J. Phys. D: Appl. Phys.* **45** 033001
- [3] Martina L W, Chuc Y H and Ramesh R 2010 Advances in the growth and characterization of magnetic, ferroelectric, and multiferroic oxide thin films *Mater. Sci. Eng. R* **68** 89
- [4] la O G J, Ahn S J, Crumlin E, Orikasa Y, Biegalski M D, Christen H M and Shao-Horn Y 2010 Catalytic activity enhancement for oxygen reduction on epitaxial perovskite thin films for solid-oxide fuel cells *Angew. Chem., Int. Ed.* **49** 5344
- [5] Jeon H, Bi Z, Choi W S, Chisholm M F, Bridges C A, Paranthaman M P and Lee H N 2013 Orienting oxygen vacancies for fast catalytic reaction *Adv. Mater.* **25** 6459
- [6] Kubicek M, Cai Z, Ma W, Yildiz B, Hutter H and Fleig J 2013 Tensile lattice strain accelerates oxygen surface exchange and diffusion in  $\text{La}_{1-x}\text{Sr}_x\text{CoO}_{3-\delta}$  thin films *ACS Nano* **7** 3276
- [7] Liu J, Collins G, Liu M, Chen C, He J, Jiang J and Meletis E I 2012 Ultrafast oxygen exchange kinetics on highly epitaxial  $\text{PrBaCo}_2\text{O}_{5+\delta}$  thin films *Appl. Phys. Lett.* **100** 193903
- [8] Bovo L, Moya X, Prabhakaran D, Soh Y-A, Boothroyd A T, Mathur N D, Aeppli G and Bramwell S T 2014 Restoration of the third law in spin ice thin films *Nat. Commun.* **5** 3439
- [9] Leusink D P, Coneri F, Hoek M, Turner S, Idrissi H, Van Tendeloo G and Hilgenkamp H 2014 Thin films of the spin ice compound  $\text{Ho}_2\text{Ti}_2\text{O}_7$  *APL Mater.* **2** 032101
- [10] Gutiérrez-Llorente A, Joross H, Woll A, Holtz M E, Ward M J, Sullivan M C, Muller D A and Brock J D 2015 Epitaxial crystals of  $\text{Bi}_2\text{Pt}_2\text{O}_7$  pyrochlore through the transformation of  $\delta\text{-Bi}_2\text{O}_3$  fluorite *APL Mater.* **3** 036105
- [11] Fujita T C, Uchida M, Kozuka Y, Sano W, Tsukazaki A, Arima T and Kawasaki M 2016 All-in-all-out magnetic domain wall conduction in a pyrochlore iridate heterointerface *Phys. Rev. B* **93** 064419
- [12] Gardner J S, Gingras M J P and Greedan J E 2010 Magnetic pyrochlore oxides *Rev. Mod. Phys.* **82** 53
- [13] Bramwell S T and Gingras M J P 2001 Spin ice state in frustrated magnetic pyrochlore materials *Science* **294** 1495
- [14] Balents L 2010 Spin liquids in frustrated magnets *Nature* **464** 199
- [15] Gingras M J P and McClarty P A 2014 Quantum spin ice: a search for gapless quantum spin liquids in pyrochlore magnets *Rep. Prog. Phys.* **77** 056501
- [16] Wang R F *et al* 2006 Artificial 'spin ice' in a geometrically frustrated lattice of nanoscale ferromagnetic islands *Nature* **439** 303
- [17] Ladak S, Read D E, Perkins G K, Cohen L F and Branford W R 2010 Direct observation of magnetic monopole defects in an artificial spin-ice system *Nat. Phys.* **6** 359
- [18] Mengotti E, Heyderman L J, Rodríguez A F, Nolting F, Hügli R V and Braun H-B 2011 Real-space observation of emergent magnetic monopoles and associated Dirac strings in artificial kagome spin ice *Nat. Phys.* **7** 68
- [19] Morgan J P, Stein A, Langridge S and Marrows C H 2011 Thermal ground-state ordering and elementary excitations in artificial magnetic square ice *Nat. Phys.* **7** 75
- [20] Kapaklis V, Arnalds U B, Farhan A, Chopdekar R V, Balan A, Scholl A, Heyderman L J and Hjörvarsson B 2014 Thermal fluctuations in artificial spin ice *Nat. Nanotechnol.* **9** 514
- [21] Gardner J S *et al* 1999 Cooperative paramagnetism in the geometrically frustrated pyrochlore antiferromagnet  $\text{Tb}_2\text{Ti}_2\text{O}_7$  *Phys. Rev. Lett.* **82** 1012
- [22] Mirebeau I, Goncharenko I N, Cadavez-Peres P, Bramwell S T, Gingras M J P and Gardner J S 2002 Pressure-induced crystallization of a spin liquid *Nature* **420** 54
- [23] Molavian H R, Gingras M J P and Canals B 2007 Dynamically induced frustration as a route to a quantum spin ice state in  $\text{Tb}_2\text{Ti}_2\text{O}_7$  via virtual crystal field excitations and quantum many-body effects *Phys. Rev. Lett.* **98** 157204
- [24] Chapuis Y, Yaouanc A, Dalmas de Réotier P, Marin C, Vanishri S, Curmoe S H, Văju C and Forget A 2010 Evidence from thermodynamic measurements for a singlet crystal-field ground state in pyrochlore  $\text{Tb}_2\text{Sn}_2\text{O}_7$  and  $\text{Tb}_2\text{Ti}_2\text{O}_7$  *Phys. Rev. B* **82** 100402
- [25] Gaulin B D, Gardner J S, McClarty P A and Gingras M J P 2011 Lack of evidence for a singlet crystal-field ground state in the magnetic pyrochlore  $\text{Tb}_2\text{Ti}_2\text{O}_7$  *Phys. Rev. B* **84** 140402
- [26] Bonville P, Gukasov A, Mirebeau I and Petit S 2014 Towards a model of a dynamical Jahn–Teller coupling at very low temperatures in  $\text{Tb}_2\text{Ti}_2\text{O}_7$  *Phys. Rev. B* **89** 085115
- [27] Fennell T, Kenzelmann M, Roessli B, Haas M K and Cava R J 2012 Power-law spin correlations in the pyrochlore antiferromagnet  $\text{Tb}_2\text{Ti}_2\text{O}_7$  *Phys. Rev. Lett.* **109** 017201
- [28] Petit S, Bonville P, Robert J, Decorse C and Mirebeau I 2012 Spin liquid correlations, anisotropic exchange, and symmetry breaking in  $\text{Tb}_2\text{Ti}_2\text{O}_7$  *Phys. Rev. B* **86** 174403
- [29] Fritsch K, Ross K A, Qiu Y, Copley J R D, Guidi T, Bewley R I, Dabkowska H A and Gaulin B D 2013 Antiferromagnetic spin ice correlations at  $(1/2, 1/2, 1/2)$  in the ground state of the pyrochlore magnet  $\text{Tb}_2\text{Ti}_2\text{O}_7$  *Phys. Rev. B* **87** 094410
- [30] Guitteny S, Robert J, Bonville P, Ollivier J, Decorse C, Steffens P, Boehm M, Mutka H, Mirebeau I and Petit S 2013 Anisotropic propagating excitations and quadrupolar effects in  $\text{Tb}_2\text{Ti}_2\text{O}_7$  *Phys. Rev. Lett.* **111** 087201
- [31] Benton O, Sikora O and Shannon N 2012 Seeing the light: experimental signatures of emergent electromagnetism in a quantum spin ice *Phys. Rev. B* **86** 075154
- [32] Bovo L and Bramwell S T 2013 Determination of the entropy via measurement of the magnetization: application to the spin ice  $\text{Dy}_2\text{Ti}_2\text{O}_7$  *J. Phys. Condens. Matter* **25** 356003
- [33] Gingras M J P, den Hertog B C, Faucher M, Gardner J S, Dunsiger S R, Chang L J, Gaulin B D, Raju N P and Greedan J E 2000 Thermodynamic and single-ion properties of  $\text{Tb}^{3+}$  within the collective paramagnetic-spin liquid state of the frustrated pyrochlore antiferromagnet  $\text{Tb}_2\text{Ti}_2\text{O}_7$  *Phys. Rev. B* **62** 6496
- [34] Mirebeau I, Bonville P and Hennio M 2007 Magnetic excitations in  $\text{Tb}_2\text{Sn}_2\text{O}_7$  and  $\text{Tb}_2\text{Ti}_2\text{O}_7$  as measured by inelastic neutron scattering *Phys. Rev. B* **76** 184436
- [35] Bonville P, Mirebeau I, Gukasov A, Petit S and Robert J 2011 Tetragonal distortion yielding a two-singlet spin liquid in pyrochlore  $\text{Tb}_2\text{Ti}_2\text{O}_7$  *Phys. Rev. B* **84** 184409
- [36] Fennell T *et al* 2014 Magnetoelastic excitations in the pyrochlore spin liquid  $\text{Tb}_2\text{Ti}_2\text{O}_7$  *Phys. Rev. Lett.* **112** 017203

- [37] Ruminy M, Bovo L, Pomjakushina E, Haas M K, Stuhr U, Cervellino A, Cava R J, Kenzelmann M and Fennell T 2016 Sample independence of magnetoelastic excitations in the rare-earth pyrochlore  $\text{Tb}_2\text{Ti}_2\text{O}_7$  *Phys. Rev. B* **93** 144407
- [38] Ruminy M *et al* 2016 First principles calculation and experimental investigation of lattice dynamics in the rare earth pyrochlores  $\text{R}_2\text{Ti}_2\text{O}_7$  (R = Tb, Dy, Ho) *Phys. Rev. B* **93** 214308
- [39] Harris M J, Bramwell S T, Holdsworth P C W and Champion J D M 1998 Liquid–gas critical behavior in a frustrated pyrochlore ferromagnet *Phys. Rev. Lett.* **81** 4496
- [40] Fukazawa H, Melko R G, Higashinaka R, Maeno Y and Gingras M J P 2002 Magnetic anisotropy of the spin-ice compound  $\text{Dy}_2\text{Ti}_2\text{O}_7$  *Phys. Rev. B* **65** 054410
- [41] Prabhakaran D and Boothroyd A T 2011 Crystal growth of spin-ice pyrochlores by the floating-zone method *J. Cryst. Growth* **318** 1053